High-contrast imaging of protoplanetary disks

Boer, J. de

Chapter 1

Introduction

1.1 How do planetary systems form?

In everyday life it may be easy to take the existence of the Earth, the Sun and all of its surrounding planets for granted. However it is among the oldest philosophical questions how they came into existence. If we consider our Solar system to be unique, then only few scientific investigations can be helpful in answering this question: we can remotely observe the bodies in the Solar system such as the planets, comets and asteroids; we can attempt daring missions to visit them (such as the Rossetta mission to visit comet 67P); or we can study the occasional meteorite, which survived its fall through the Earth's atmosphere. But the most helpful observations will never be performed: observations of the Solar system as it was in its very beginning, about 4.6 billion years ago (based on the ratio of lead isotopes within meteorites, Bouvier & Wadhwa 2010).

Even though we cannot go back in time to observe the young Solar system, the German Philosopher Immanuel Kant has shown that it is possible to investigate the origin of our planetary system by combining observations of the current Solar system with philosophical reasoning. Kant (1755) starts out with two conflicting observations:

1. The planets within the Solar system appear to be orbiting in the same direction and within the same plane, which hints at a common cause for their movement and position.

2. Most of the Solar system is empty, seemingly excluding the possibility of a driving force behind the commonality in motion and location.

From these two observations he arrives at what is now known as the 'Nebular Hypothesis'[1]: during the formation of the Solar system, the space it currently occupies cannot have been as empty as it is today, but rather be "filled with matter sufficiently powerful to transmit motion onto all the heavenly bodies contained in it". This matter is the same as what composes the Solar system today, but dispersed more evenly as an enormous cloud. Within the dispersed nebula, a region with enhanced density will start to attract surrounding matter from which this dense core will start growing. Although all matter surrounding it will fall towards the growing core, some will be "deflected" from its free-fall and arrive at a circular orbit. Initially the combined circular orbits of the surrounding matter will form a three dimensional shape, but they will eventually flatten into a disk. Within this disk, new clumps of larger density will emerge. Matter surrounding such clumps is orbiting with roughly the same velocity. Therefore, the relative motion of this nearby material is small enough to be accreted onto the newly forming clumps. The most massive central core will grow to become the Sun, which will eventually acquire its "flaming heat that brakes out upon its surface". Meanwhile the accreting clumps will grow to become planets, which will continue on the initial orbits of the clumps.

Kant does not stop at explaining just the formation of the Solar system, but extrapolates his hypothesis to all stars:

> "All the fixed stars that the eye discovers in the hollow depth of the heavens and that appear to demonstrate a kind of extravagance, are suns and centre points of similar systems. The analogy thus does not permit any doubt here that these were formed and generated in the same manner as the one in which we find ourselves..."

We can also reverse the direction in which Kant studied the formation of the Solar system. Since not all stars surrounding us have formed during the same time, we can learn the general principles behind the formation of planetary systems by studying stars and extrasolar (planetary) systems that are currently being formed. If, like Kant, we consider the possibility that our Solar system has formed in a manner comparable to systems which are currently in formation, then this study also becomes relevant for understanding the history of our own Solar system, of the Earth and eventually ourselves.

In the last few decades, we have detected many planets in orbit around stars other than our Sun (i.e. extrasolar planets or exoplanets) as well as circumstellar matter such as gas and solid particles (dust) around young stars still in formation. If we paint the picture of our current understanding of star and planet formation, it is astonishingly similar to the picture painted by Kant. We might argue about

[1] which is possibly inspired by the work of Emanual Swedenborg in his 'Opera Philosophica et Mineralia', published in 1734.

several of Kant's driving mechanisms behind the formation. Still, his essential idea of starting out with a roughly homogeneous nebula that collapses into a dense core, surrounded by a disk out of which the planets form, is the same.

Because of recent advancements in astronomical instrumentation, many aspects of what we study in the field of planet formation are seen for the first time. This poses the natural question of whether the new discoveries reveal a general step in planet formation, common in the formation of all extrasolar systems; or whether we have found a rare and extreme phenomenon that only happens in exceptional cases. The picture we can currently draw of the formation of planetary systems contains much more detail than the picture drawn by Kant, yet we are often still surprised by our observations of particular details, which can require us to go back to the drawing board.

In the remainder of this section, I will give a broad outline of our current understanding of the formation of planetary systems; the subsequent sections will describe several open questions and the methods with which we aim to answer them. I conclude this chapter with an outline of how I contributed to answering these questions during my Ph. D. research project.

1.1.1 From molecular clouds via globules to disks

Much of the early formation stages of an extrasolar system is an interplay between the circumstellar matter and the star it surrounds. In the very first stage, no distinction can be made between the two. We start with the classical picture of star formation with a giant molecular cloud (GMC, e.g., the Eagle Nebula in Figure 1.1 a), which typically contains a total mass between a thousand and up to tens of million times the mass of the Sun (hereafter: solar mass or $M_\odot$). The mass of a GMC is mostly made up of molecular hydrogen (H_2) gas, although more complex molecules are detected, such as Polycyclic Aromatic Hydrocarbons (PAHs, van Dishoeck 2004). Dust grains are already present and form the primordial building blocks needed to eventually form planets.

When a GMC becomes gravitationally unstable it fragments and collapses to form the first high-mass stars (tens of solar masses). The large radiation pressure originating from these bright, massive stars cause further fragmentation of the molecular cloud. Notice how the pillars (or columns) of gas and dust in Figure 1.1 a point away from the massive stars. The radiation cleans the region surrounding the massive stars from the inside-out, which allows a local overdensity in the nebula to cast a shadow outward, thus creating a pillar. The pillars are affected by the destructive forces of both the intense radiation of the massive stars and shock waves due to supernova explosions from the abrupt death of the short-lived, massive stars.

In 1908, Barnard detected dark regions against the bright background of

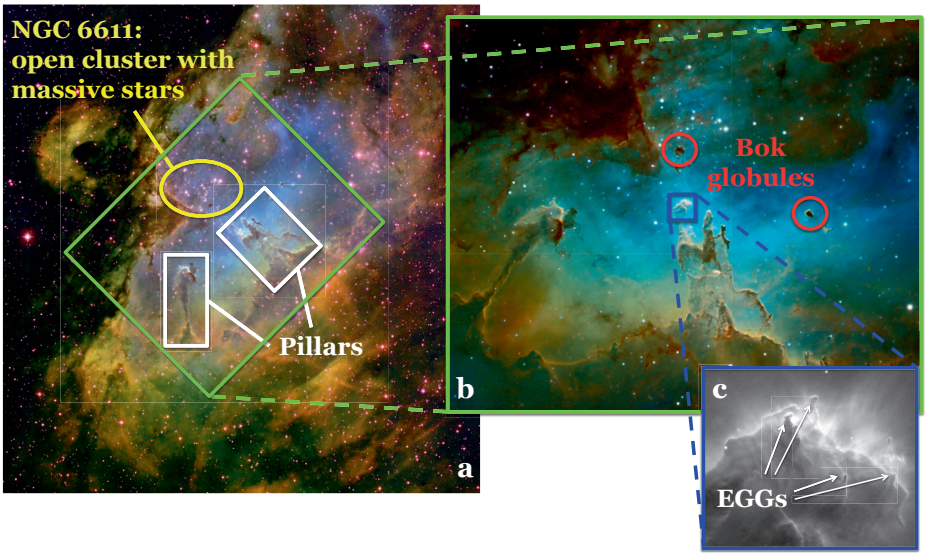

Figure 1.1: Pillars, Bok globules and Evaporating Gaseous Globules (EGGs) in the Eagle Nebula (M16). Courtesy wide field (a): T.A. Rector & B.A. Wolpa (NOAO/AURA/NSF); first zoomed region (b): Emanuele Colognato & Jim Wood (APOD) and smallest field (c): J. Hester and P. Scowen (AZ State University), NASA.

the Lagoon Nebula, which he described as "a number of very black, small, sharply defined spots or holes". These small, dark spots were named globulae and recognized by Bok & Reilly (1947) as nebulae that "probably represent the evolutionary stage just preceding the formation of a star". Globulae (or globules) are believed to be cores of higher density that survived their violent surroundings, either liberated from (Bok globules, Figure 1.1 b) or still attached to the pillars (Evaporating Gaseous Globules or EGGs, Figure 1.1 c). The review of Bergin & Tafalla (2007) describes how the low temperatures in the dark globules form an ideal starting point for the growth of dust grains. Complex molecules freeze out onto the sub-micron sized dust grains, giving the grains icy mantles. These mantles allow the grains to coagulate (Lazarian et al. 1997) and grow to larger sizes.

The regions of the highest density within these globules or molecular cores contract to form 'protostars'. The dense gas and dust within globules shield the protostar, making it invisible at short wavelengths; the protostar is *embedded* within its native nebula or envelope. In the earliest, most embedded stages,

protostars are only visible at (sub)millimeter wavelengths. As soon as the material of the envelope surrounding the protostar is accreted or dispersed, the now visible object is called a pre-main sequence star.

A generic term for (proto)stars in formation is Young Stellar Object (YSO). Lada (1987) suggested a classification of YSOs based on the spectral index (= the derivative of the energy distribution) of the YSOs:

$$\alpha_{\rm IR} = \frac{d\log(\lambda F_\lambda)}{d\log(\lambda)}, \tag{1.1}$$

for wavelengths (λ) between 2 and 25 micron (μm). In this equation, F_λ is the (spectral) flux density, while λF_λ yields the flux: the amount of radiation energy passing through (or measured over) a surface area per unit time. Lada specified three categories: class I ($\alpha_{\rm IR} > 0$); class II ($-2 \lesssim \alpha_{\rm IR} \leq 0$); and class III ($\alpha_{\rm IR} \lesssim -2$). These classes were linked to the subsequent evolutionary stages of protostars and the more evolved pre-main sequence stars by Adams et al. (1987), who also added the Flat Spectra class (FS, Adams et al. 1988) as category in-between Class I & II. Additionally, Andre et al. (1993) introduced Class 0 for the most embedded protostars within globules, based on millimeter (mm) observations. The characteristics of the five classes of YSOs and the currently used values for the spectral indices are listed in Table 1.1.

1.1.2 From protoplanetary disks to planetary systems

Yorke et al. (1993) have modeled how a molecular core collapses into a protostar and within approximately ten thousand years into a circumstellar disk. The gas and dust from the surrounding nebula (or envelope) slowly accretes onto the disk or evaporates due to the extremely high luminosity of the protostar (i.e. photoevaporation), at which time the globule evolves (Hester et al. 2004) into a photoevaporating protoplanetary disk (or proplyd, see Figure 1.2). This continuous evaporation and accretion dissipates the envelope, which starts displaying cavities in the polar region during the YSO FS class (Calvet et al. 1994).

Finally, the envelope is dispersed completely and the pre-main sequence star becomes visible, surrounded by a protoplanetary disk. The pre-main sequence star is called a T Tauri star (for a stellar mass $M_\star \lesssim 2M_\odot$) or a Herbig Be/Ae star (for $M_\star \gtrsim 2M_\odot$). During the Class II phase, the optically thick disk is accreting onto the star, which becomes apparent from strong hydrogen line (Hα, at 656 nm) and ultraviolet (UV) emission. T Tauri stars with strongly accreting disks are called Classical T Tauri Stars (CTTS) and are recognized by the strength of the Hα emission line (White & Basri 2003). The protoplanetary disks around Class II YSOs are often called primordial.

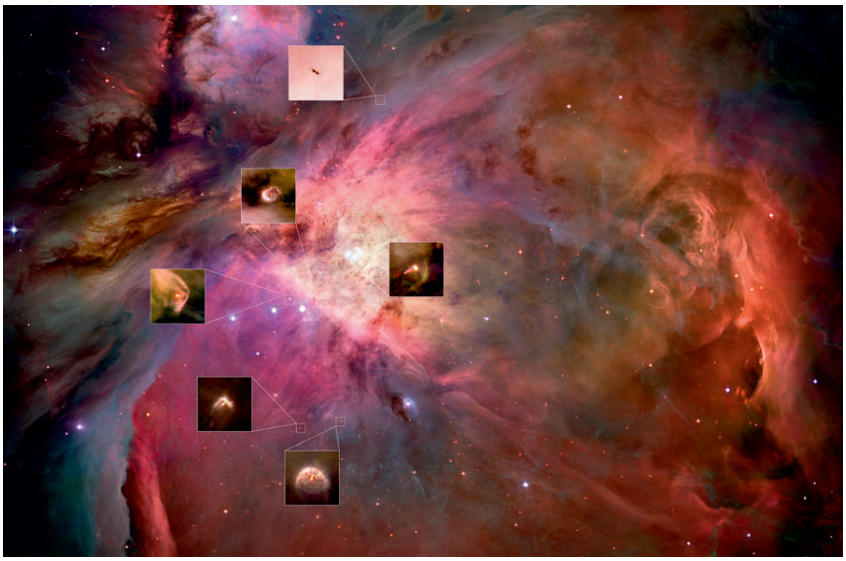

Figure 1.2: Photoevaporating protoplanetary disks or *proplyds* in the Orion Nebula. Courtesy: NASA, ESA, M. Robberto (STScI/ESA), the HST Orion Treasury Project Team, & L. Ricci (ESO)

1.1.2.1 From dust to planets

Throughout the disk evolutionary stages, dust grains continue growing in size. While the distribution of small (< mm) grains is tracing the gas density, the larger grains decouple from the gas disk. Instead, large grains are drawn towards (even slight) local pressure maxima in the gas, which can create a large grain distribution that deviates strongly from the gas (and small dust) density distribution. Due to a radial gas pressure gradient, the gas disk orbits the star at velocities just below Keplerian, which creates drag felt by the large grains, which are on Keplerian orbit (Weidenschilling 1977). This headwind slows the large particles down and causes an inward migration (or "radial drift") of these grains. Additionally, vertical gas pressure gradients will cause the larger grains to move (settle) towards the mid-plane of the disk (D'Alessio et al. 1999). Meanwhile, small grains remain radially and vertically mixed. For dust to grow into rocks, planetesimals and finally planets, the growth has to occur before the large grains have migrated inward towards the star to regions so hot that dust turns into gas (inside the "dust sublimation radius"). Unperturbed radial drift would move meter-sized bodies from 1 au separation into the sublimation radius in the order of a hundred years (Brauer et al. 2008). To allow further growth, large dust

grains have to halt their inward migration either by growing very quickly into sizes no longer sensitive to the gas drag (the drift for 10 m objects is already ~ 10 times slower than for 1 m sized particles), or due to different mechanisms such as "dust trapping" in local pressure maxima.

Terrestrial (rocky) planets grow according to the previous description of grain growth. Contrary to the formation of rocky planets, gas giant planet formation can carve gaps in the gas (and subsequently dust) disk. Giant planets need to acquire their sizable gaseous envelopes for which two models are most commonly considered. According to the core accretion model (Pollack et al. 1996), giant planets start runaway accretion of the surrounding gas once the solid planetary cores have reached a critical mass of roughly ten Earth masses. Growth of the gaseous envelope continues until all gas within gravitational reach of the planet has been accreted or until the gas disk is evaporated by stellar radiation. A major problem with this model is that the time expected to be necessary for a planetary core to reach critical mass equals or exceeds the typical lifetime of the gas disk. The details of grain growth are not well understood. Freeze-out of molecules onto the dust, allowing coagulation can explain grain growth up to mm-sized grains. However, collisions between dust/pebble sizes from a centimeter to a meter are more likely to result in fragmentation of the particles rather than the creation of even larger bodies (Blum & Wurm 2008). Alternatively, the gravitational instability model assumes that giant planets form in the disk the same way as protostars form in molecular cores: by means of gravitational collapse of the parent body (Boss 1997). Massive disks can become gravitationally unstable, causing the protoplanetary disk to fall apart into self-gravitating fragments. These fragments will form giant planets at timescales much shorter than the core accretion model does. However, for gravitational collapse to occur, the disk should be able to cool down on orbital timescales, which is much faster than expected.

1.1.2.2 Transitional and debris disks

As time progresses, depletions (often called holes or cavities) in the dust disk form close to the star, effectively stopping accretion onto the star. Strom et al. (1989) first recognized these disks with inner cavities by a dip in the near-infrared (NIR) part of their spectral energy distribution (SED), and named them *disks in transition* from primordial accreting into tenuous debris disks. The inner clearings in the dust of a transition disk may have multiple possible origins, such as photoevaporation by the central star (which would clear the disk inside-out, Chiang & Murray-Clay 2007, Hollenbach et al. 2000); dust trapping at a pressure maximum caused by dead zones (disk regions with low ionization rate, making it insensitive to magnetic fields, Gammie 1996); or trapping in a pressure

YSO	System	SED slope*	Physical properties	Observational prop.	Timescales**
0	globule		$M_{env} > M_{star} > M_{disk}$: protostar & disk are embedded in thick envelope	No emission at $\lambda < 20\,\mu m$	Disk forms in $t_0 \leq 10^4$ years
I	globule/ proplyd	$\alpha_{IR} > 0.3$	$M_{star} > M_{env} \sim M_{disk}$: envelope disperses during this phase	Generally optically obscured	$t_0 \leq t_I \leq$ 0.5 Myr
FS	proplyd /CTTS	$-0.3 < \alpha_{IR} < 0.3$	Invall from envelope remains, except from polar cavities in envelope.	Inbetween Class I and II	$1 \sim 10$ Myr
II	CTTS primordial	$-1.6 < \alpha_{IR} < -0.3$	$M_{star}/M_{disk} \sim 1\%$, $M_{env} \sim 0$: Accreting disk	Strong Hα & UV emission	$t_I \leq t_{II} \leq$ $1 \sim 10$ Myr
III	WTTS transition /debris	$\alpha_{IR} < -1.6$	$M_{star}/M_{disk} \ll 1\%$, $M_{env} \sim 0$: Passive disk: no or weak accretion	SED dips in NIR regime	$t_{II} \leq t_{III} \leq$ $t_{II} + 0.5$ Myr***

Table 1.1: Adapted from Table 1 and main text of Williams & Cieza (2011). *) α_{IR} is the slope of the Spectral Energy Distribution (SED) for $2 \leq \lambda \leq 25\,\mu m$. **) Note that the ages are given for solar type and lower mass stars and are $\sim 2\times$ shorter for disks around higher mass stars due to higher accretion rates and more violent radiation. The ages should be considered as an indication since studies based on IR excess surveys are plagued by large uncertainties in the stellar age estimates. Additionally, the disk lifetime depends strongly on factors as how crowded the surrounding field is with neighboring stars. ***) This age refers to the time scale for dissipation of gas after accretion has stopped (Cieza et al. 2007).

maximum created by the clearing of inner disk regions by massive planetary companions, via core accretion (Calvet et al. 2002). Furthermore, Espaillat et al. (2007) introduced the class of *pre-transitional disks* to describe systems where the dip in the SED is preceded (at shorter wavelengths) by a substantial NIR excess, which hints at an inner disk separated from the colder outer disk. A gap (instead of a cavity) in the disk can no longer be caused by photoevaporation (as this inside-out process will remove the inner disk first), which therefore makes clearing by massive companion the more likely cause for the gap. Espaillat et al. suggest that the inner disk of a pre-transitional disk eventually clears, changing the disk into a transition disk. Whether all transition disks are preceded by pre-transitional disks, or whether alternative clearing mechanisms can create large holes without the initial creation of a gap is not yet clear.

Eventually, most of the dust will grow to larger sizes and settle to the disk mid-plane. After the gas and dust of the inner disk has accreted onto the star, the gas and remaining small particles in the outer disk will gradually evaporate, making the disk more tenuous and therefore optically thin for the light of the central star (Alexander et al. 2006). The collision of larger particles will create second-generation small dust particles (debris). Disks where the gas has (almost) completely evaporated are therefore known as *debris disks*. The absense of gas and low density of the dust disk make it unlikely that giant planets will still form

within debris disks.

Low mass pre-main sequence stars where accretion is absent (i.e. the Hα emission line is 'weak') are called Weak-lined T Tauri Stars (WTTSs), which could either encompass systems with transition disks, debris disks or no disk at all. These stars continue to contract until the temperature at the stellar core is sufficient for hydrogen fusion to start, while the dust in the disk is mainly grouped into thin rings or (asteroid) belts around the star (Wyatt 2008). With the start of hydrogen fusion the star enters 'adulthood' known as the Main Sequence (MS), which is the current state of our Solar system.

1.1.3 Herbig Be/Ae Stars

George Herbig was the first to attempt to find the precursors of intermediate mass (2 - 8 $M_\odot$) MS stars of spectral type Be and Ae. Herbig (1960) presented "a list of 26 Be- and Ae- type stars that both lie in obscured regions and illuminate nearby nebulosity". Although Herbig does not rule out that some members of the list are indeed pre-main sequence, he cannot find sufficient, unique spectroscopic features that clearly distinguish the list from a general sample of stars with the same spectral type. Nonetheless, we now know that all members of this list are in fact pre-main sequence stars, which made this list a standard catalogue. Therefore, pre-main sequence stars with masses above 2 $M_\odot$ became known as Herbig Be/Ae stars.

Because of the high luminosities of their parent stars, the disks around Herbig Be/Ae are subject to higher irradiation and therefore more prone to photoevaporation than disks around low mass T Tauri stars. The Herbig disks are also hotter for similar separations from the star and are brighter in emitted as well as reflected light. Primordial disks are in hydrostatic equilibrium (Kenyon & Hartmann 1987), meaning that the gas pressure is in equilibrium with gravity. We expect that for most disks dust particles are in a Keplerian orbit around the star, and the dominant component of gravity is the vertical component (towards the disk mid-plane) of the stellar gravity. The horizontal (radial) component of the stellar gravity is counter-balanced by the centrifugal force of the Keplerian rotation. Since the vertical component of the gravity decreases with separation from the star (or disk radius r) the pressure scale height H (height above the mid-plane where the pressure has decreased with a factor of e) of a primordial disk generally increases with r.

A classification of Herbig stars was proposed by Meeus et al. (2001) between sources for which the SED can be fitted with either only a power law (group II) or a power law together with the spectrum of a black body (group I). Additionally, a subdivision was made between spectra displaying the presence (group Ia/IIa) or absence (group Ib) of solid-state bands (e.g., silicate lines). Meeus et al.

interpret group Ia/b disks as being strongly flared (non-linear increase of disk scale height H with disk radius r), while group IIa disks are non-flaring (H/r is constant, sometimes called "flat"). When the inner edge of the dust disk becomes "puffed-up"[1] due to intense stellar radiation, the outer regions of a non-flaring disk will lie in the shadow of the thick inner rim. Such self-shadowing will not occur for flaring disks (except possibly right behind the puffed-up rim), allowing the surface of the outer regions of a flaring disk to absorb and scatter starlight.

Furthermore, Meeus et al. (2001) suggest an evolutionary hierarchy: flared disks eventually cool down (decreasing the pressure) and become flat. This scenario might sound plausible: disks do cool down over time, and growing dust grains will eventually settle towards the disk mid-plane. However, the theory of flared group I disks evolving into flat group II disks is challenged by radiative transfer modeling of silicate features in group I disks by Maaskant et al. (2013). The absence of the silicate features in group Ib is explained by Maaskant et al. by including a large gap in the disk, which covers the region where these features originate. Group IIb objects (possibly non-flaring disks with a gap of similar size as the group Ib disks) have never been detected to date, suggesting that no (or at least very few) group II disks have gaps as large as the group Ib sources. I discussed in Section 1.1.2 how gaps are formed in pre-transitional disks and are considered to be tracers of advanced evolution; hence disks with larger gaps are in general more evolved than disks with smaller or no gaps. Therefore, it is unlikely that group II disks have evolved from group I sources.

1.1.4 Primordial versus transition disks

Transition disks are rich in large-scale structure. Their most distinct feature is the inner clearing in the dust disks (see Section 1.1.2.2) as can clearly be seen in the image of RX J1604.3-2130A (J1604) in Figure 1.3a (a detailed study of this object is given in Chapter 3). Yet additional features such as spiral arms (see Figure 1.3b) and azimuthal asymmetries tracing dust trapping vortices (see Figure 1.3c) are often apparent in transition disks. Probably all three examples of large-scale features are somehow related to the growth of dust grains from sub-micron size to (at least) millimeter size. Inefficient fragmentation of large grains at specific disk radii can cause a lower abundance of small grains at these radii, resulting in apparent annular depressions in scattered light images (Birnstiel et al. 2015).

[1] The inner rim of the dust disk is irradiated under small angles of incidence, while the disk surface at larger radii will be irradiated at grazing angles of incidence. The more efficient irradiation at small angles causes the disk to heat-up (and increase the gas-pressure) more efficiently at the rim than at larger radii (Calvet et al. 1991), making a puffed-up inner rim of the disk more likely than puffing-up for regions at larger r (Dullemond et al. 2001).

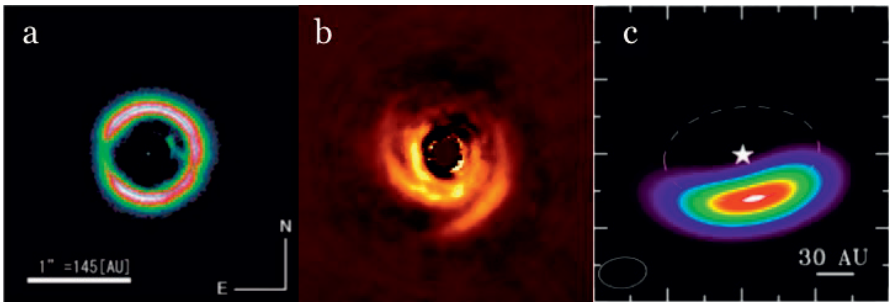

Figure 1.3: Three transition disks. **a)** RX J1604.3-2130A imaged in polarized intensity with SUBARU/HiCIAO from Mayama et al. (2012). **b)** SAO 206462 detected with Magellan/Magao/Clio2 with reference star subtraction (RDI) from Ménard, de Boer et al. in preparation. **c)** ALMA cycle 0 image of IRS 48 from van der Marel et al. (2013).

The most prominent theories suggest that cavities and gaps are often cleared and spiral arms often dragged along by orbiting planets, the end result of grain growth. The initially axi-symmetric traps of mm-sized dust in pressure maxima in the disk can harbor Rossby wave instabilities (Lovelace & Romanova 2014), responsible for the asymmetrical vortices we see in IRS 48 (van der Marel et al. 2013) and HD 142527 (Casassus et al. 2013), while the smaller (μm) grains do not experience this trapping by gas pressure maxima as strongly as the mm-sized grains.

The details of large-scale structure formation within the disk remain the subject of debates. Montesinos et al. (2016) discuss how shadows cast by an inner disk, possibly aided by self-gravity, can trigger spiral waves in the outer disk without the necessary presence of planets. This explanation begs the question whether the observed large-scale features are induced by variations in the gas pressure field or in the gas and dust density field. The realization that flared disks can in fact be (pre)-transitional put our understanding of the evolution of protoplanetary disks into question, as discussed in Section 1.1.3. Yet another puzzling discovery was obtained when the Atacama Large Millimeter Array (ALMA) tested its long baseline by observing HL Tauri (see Figure 1.4). This star is believed to be very young ($\sim$ 0.5 million years or Myr) and still has a primordial disk. However, the ALMA press release sub-mm continuum image (ALMA Partnership et al. 2015) surprised the planet-formation community by showing strong gaps in the disk surface density. These features were previously thought to be an evolutionary trait of the (pre-)transitional disks, which are typically much older. In fact, it is suggested that the gaps in the disk of HL Tau

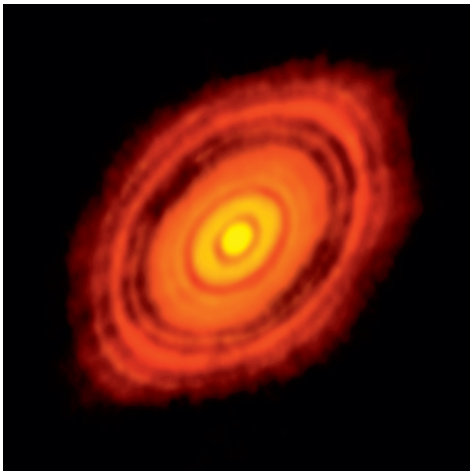

Figure 1.4: ALMA long baseline image of HL Tau (ALMA Partnership et al. 2015).

can be ascribed to the presence of planets (Pinte et al. 2016, Takahashi & Inutsuka 2016), which would indicate that planets can form much faster than the core-accretion theory predicts.

1.2 Current understanding of disk evolution

Our general understanding of the formation of solar systems as outlined in Sections 1.1.1 & 1.1.2 shows striking similarities with the nebular theory as hypothesized by Immanuel Kant (Section 1.1). One might wonder whether our understanding has advanced during the last 250 years. However, it is one thing to propose a hypothesis; it can sometimes be far more complicated to corroborate it to form a credible theory. Additionally, in the more intuitive hypothesis of Kant, the underlying physics is often wrong, while in the current age of radiative transfer, dynamical and chemical modeling the physics of these systems is either well understood or an active field of research. In short, contrary to Kant we have a far better overview of what we do and do not know. It turns out that as is often the case, the 'devil is in the details'. This thesis focusses on the study of primordial and transitional disks (Class II & early III YSOs). From the discussion in Section 1.1 we determine the most urgent outstanding questions in this field of research.

1.2.1 Open questions

Many questions remain in the study of protoplanetary disks. A selection of currently unanswered questions is given below, based on their relevance for the studies included in this thesis.

1. How do grains grow beyond cm sizes? Can the core accretion model fully explain the gradual growth of small grains into ever increasing sizes up to planetary cores, or do we need alternative explanations such as a streaming instability (Blum & Wurm 2008, Youdin & Goodman 2005)?
2. What is the nature of rings, gaps and spiral arms? Are they formed by variations in the density field or are they due to spatial temperature / pressure fluctuations?
3. Different large-scale structures can be attributed to the same cause. For example both spiral arms and annular gaps and rings can be explained by the presence of planets. Rings are detected in disks of both young (HL Tau) and relatively old (TW Hya, see Andrews et al. (2016)) stars. The circumstances under which a disk will form specific large-scale structures are still not unambiguously determined, making it difficult to constrain the evolutionary stage of disks from the observed disk features.
4. Is there an evolutionary sequence from non-flaring to flaring disks, or vice versa?
5. For non-flaring or mildly flaring disks we would expect self-shadowing to occur in these protoplanetary disks. Photometric light curve measurements often show strong variability in stars with non-flaring disks. Can self-shadowing explain these variations? And can we use multi-epoch disk imaging observations to characterize the inner (unresolved) disk structures responsible for casting such shadows?

1.2.2 Finding answers to the open questions

In this section I explore how to find answers to the questions (**Q**) posed in Section 1.2.1. The explorations are listed according to the question(s) they refer to.

Q1) Ongoing grain growth can be studied in laboratory environments. Meanwhile, studying spatial variations in the dust size distribution of disks in varying evolutionary stages will show whether the dust grows gradually according to the core accretion model or whether we should expect to find features hinting at gravitational instabilities (framentation will result in radial and azimuthal variations such as spiral structures in the surface density). To

determine dust size and density distributions we need to combine radiative transfer models with sub-mm continuum imaging of the mm-sized dust as well as (preferably multi-wavelength) measurements of the degree of polarization for light scattered by the micron-sized grains. Currently available polarimetric images of protoplanetary disks provide us with the polarized intensity, which are not calibrated for polarimetric efficiency (the ratio between the incident and measured degree of polarization). To measure the degree of polarization we must measure determine the absolute polarized and total intensity profiles first. In Chapters 5 and 6 we describe the calibration of two polarimetric high-contrast imagers at the Very Large Telescope (VLT) of the European Southern Observatory (ESO) at Cerro Paranal in Chile: NAOS/Conica (VLT/NACO, Chapter 5) and the InfraRed Dual-beam Imager and Spectrograph of the SpectroPolarimetric High-contrast Exoplanet REsearch instrument (VLT/SPHERE/IRDIS, Chapter 6). These calibrations are essential if we wish to determine the absolute polarized intensity profile and use it to derive the degree of polarization.

Q2,Q3,Q4) Many of the stated questions are related to each other; finding the answer to one will aid us to answer others. The answer to question 3 about when disk features form requires us to first learn the answer to question 2 about the nature of these features. We need detailed knowledge of the geometry of the disk to distinguish between density and pressure gradients. Sub-mm imaging with ALMA and radiative transfer modeling can give us the radial dependence of scale height, while under the right circumstances (e.g., rings in the disk scattering surface) scattered light imaging can provide us the height of the scattering surface above the mid-plane, as we illustrate in Chapter 4. Determining the radial dependence of the disk height for a wide range of systems will also provide insight in which disks are and which are not flaring, which is a necessary step towards answering question 4.

Q5) Variability in the light curve of a YSO with a non-flaring disk is often interpreted as the transit of inner disk material across the line of sight. Similarly, the inner (unresolved) disk casts shadows on the outer (spatially resolvable) disk that can be variable. These shadows can be detected when we image these disks in scattered light. In Chapter 3 we describe the detection of temporal variations in the disk surface brightness of J1604. When we compare our image of the disk with previous observations, the dip in the disk ring (see Figure 1.3) moves by at least 12 degrees per year. This variation in the location of the dip can be explained by considering the dip to be a shadow that is cast by an inner disk feature. The separation from the star of this inner disk feature is much smaller than the radius of the resolved disk ring.

My contribution towards answering the questions described in the previous section consisted primarily of high-contrast imaging of protoplanetary disks in scattered light at high angular resolution. The definitive answers to

the outstanding questions will ultimately require the combination of images obtained through high-contrast imaging with modeling of radiative transfer[1] and dynamical[2] processes, and with archival and future observations taken with complementary observing modes (especially ALMA observations to detect the gas and mm-sized dust grains).

1.3 High-contrast imaging of disks in the visible and near infrared

1.3.1 The challenge posed by high-contrast

Beyond the first few astronomical units (au, which is the distance between Earth and the Sun) circumstellar disks are typically too cold to emit light at visible and NIR wavelengths. However, it does become possible to image the disk surface in these wavelength regimes when this surface scatters stellar light in the direction of Earth. The first disk that was succesfully imaged in reflected light is the debris disk around β Pictoris by Smith & Terrile (1984). To do so, Smith & Terrile needed to overcome a major problem: how to bridge the large contrast between the bright star and the faint surface brightness of the disk?

If stars would appear on the instrument detector as a point source, we could simply saturate the single pixel where the star is imaged and detect the disk image on the surrounding pixels. Unfortunately, there are several reasons why the star does not appear as a point source, but as an extended speckle halo. Even if the starlight would reach the telescope as a perfectly flat wave-front, the diameter (D) of the telescope pupil places a lower limit on the angular size of the star on the detector, called the diffraction limit ($= 1.22\lambda/D$). For a perfect imaging system, a point source will be imaged as the (absolute value squared of the) Fourier transform of the complex telescope aperture. Wave-front disturbances due to telescope and instrumental aberations (e.g. the support structures for the secondary mirror, which are often called "spiders") can create interference patterns, known as speckles. The full response of the imaging system is called the instrument's Point Spread Function (PSF).

Turbulence in the terrestrial atmosphere disturbes the wave-front and causes time-dependent speckles. Therefore, the angular resolution of the observation becomes the Full Width at Half Maximum (FWHM) of the effective PSF, which is comprised of the instrument response and the seeing term (Roddier 2004).

[1] Computes how the disk reprocesses the stellar radiation. It tells us what a disk with specific parameters will look like at a chosen wavelength.

[2] Computes how a disk evolves over time to explain the underlying cause for detected disk features and predict yet undetected features.

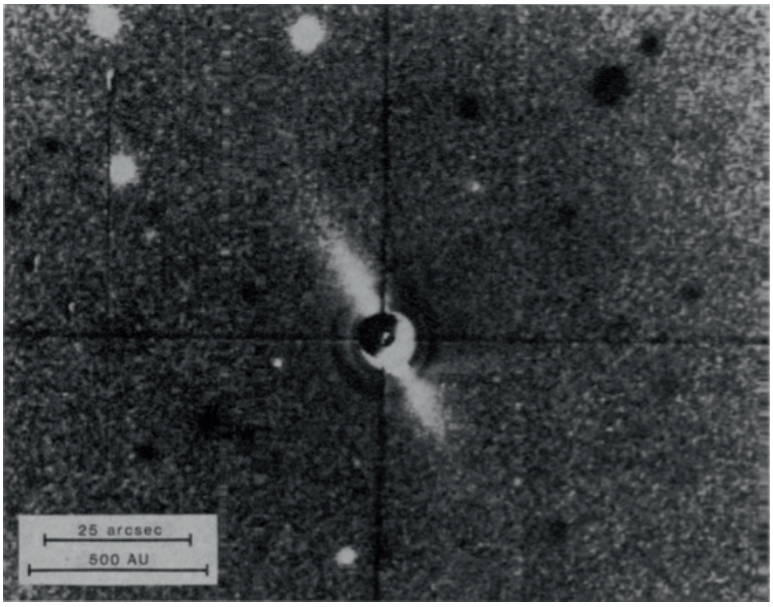

Figure 1.5: The first direct detection of a circumstellar disk: the debris disk surrounding β Pictoris. Courtesy: Smith & Terrile (1984)

1.3.2 High-contrast imaging techniques

Smith & Terrile (1984) describe two methods that they have used to remove the stellar speckle halo: 1) They used a Lyot coronagraph, which contained a focal plane mask (with an angular diameter of 7 arcseconds, where 1 arcsecond (1″) = 1°/3600) to remove the brightest peak of the PSF, and a Lyot stop to remove residual diffraction caused by this mask. 2) They imaged α Pictoris with the same instrumental setup to obtain a reference PSF, undiluted by the disk. The second step allowed the authors to perform 'PSF subtraction' on the β Pictoris image. The application of coronagraphy and PSF subtraction yielded the first detection of a circumstellar disk (see Figure 1.5).

Both coronagraphy and PSF subtraction remain essential components of modern-day high-contrast imaging. However, both techniques are impaired by the temporal variations of the PSF due to variable seeing. To circumvent the effects of the atmosphere, we can either place our imaging system outside of the atmosphere, or correct for seeing effects. Space telescopes, such as NASA's

Figure 1.6: Secondary mirror (M2) of Magellan's Clay telescope. The secondary is the deformable mirror for the Magellan adaptive optics system MagAO.

Hubble Space Telescope (HST) have the advantage of a very stable PSF and the possibility to observe faint targets with very long integration times. Unfortunately, it is expensive to launch large optical systems. Therefore, budgetary constraints limit the size of the primary mirror of space telescopes (e.g., for HST, $D = 2.4\,\mathrm{m}$), which constrain the diffraction limit.

The more affordable alternative to observing from space is to create Adaptive Optics (AO) systems for large (typically $D = 6 - 10\,\mathrm{m}$) ground-based telescopes. Recent examples of AO systems are the Keck AO system (Wizinowich et al. 2006), the NAOS (Rousset et al. 2003) system of VLT/NACO (Lenzen et al. 2003), AO188 (Hayano et al. 2010) of Subaru/HiCIAO (Tamura et al. 2006), and the currently available eXtreme AO (XAO) assisted imagers, such as Gemini/GPI (Macintosh et al. 2014), Magellan/MagAO (Close et al. 2012), and VLT/SPHERE (Beuzit et al. 2008), assisted by SAXO (Fusco et al. 2014). These AO systems all contain a deformable mirror (DM) and a tip-tilt mirror in the common path of the instrument (or telescope, e.g. Magellan/Clay's secondary mirror is the DM for the MagAO system, see Figure 1.6). A (usually dichroic) beam splitter downstream from the DM, separates the science beam (which is directed towards the science instrument and yields the scientific images) from the beam that is directed towards the AO Wave-Front Sensor (WFS). While the science detector is recording, the WFS senses (typically at much higher read-out rates than the science detector) aberations to the wave-front. A real-time computer determines how to correct the aberations and sends the corresponding commands to the DM. The DM will deform accordingly to correct for wave-front errors to create a flat wave-front, thus improving the Strehl ratio (peak of the measured PSF

divided by the peak of the ideal PSF of the system) for the science frames.

The first implication of the AO-improved Strehl ratio (and smaller FWHM of the PSF) is the higher angular resolution of the observations. However, AO has a much more important benefit than just higher resolution imaging: it allows higher contrast imaging due to the more stable (less time-variable) PSF. The stability of the PSF enhances the centering of the star behind a coronagraph mask (which can therefore be made much smaller, typical mask radii are $\sim 0.05''$ for XAO systems). Additionally: PSF subtraction becomes more reliable with a stable PSF, especially when the technique is using a PSF that is not measured simultaneously with the science frame.

1.3.2.1 PSF subtraction or differential imaging techniques

Several PSF subtraction (also known as 'differential imaging') methods exist.

- ADI: Angular Differential Imaging
- SDI: Spectral Differential Imaging
- RDI: Reference star Differential Imaging
- PDI: Polarimetric Differential Imaging

These techniques are discussed in the remainder of this section, except PDI, which is discussed in Section 1.3.3.

ADI Angular Differential Imaging (ADI, Marois et al. 2006) is currently the preferred high-contrast imaging technique to detect point sources (e.g., exoplanets). This technique uses the rotation of the field as seen by the pupil of an alt-azimuth telescope. Contrary to conventional imaging techniques it is necessary to stabilize the pupil rather than the field on the detector. In Figure 1.7 it is illustrated how in pupil tracking mode a circumstellar object (the red dot) will rotate with the parallactic angle around the central star, while the pupil (including spider structure) remains fixed on the detector. The subsequent steps for classical ADI (cADI) can be found in the figure: take the median of the science frames and subtract this median from each frame; derotate the PSF subtracted images with the parallactic angle (places north up on the image) and take the median of the derotated images.

We can replace the first median (Step 2 in Figure 1.7) by determining the best PSF using alternative post-processing routines such as Principle Component Analysis (PCA, Amara & Quanz 2012, Soummer et al. 2012), or (Template) Locally Optimized Combination of Images ((T)LOCI Lafrenière et al. 2007, Marois et al. 2014). These routines are optimized to minimize residual speckle noise but increase the risk of subtracting 'true' signal. Because the reference PSF is created

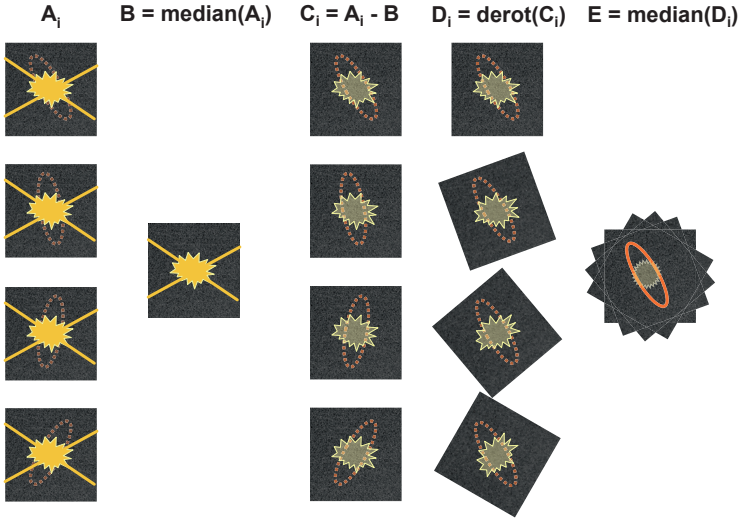

Figure 1.7: Angular Differential Imaging, courtesy: Christian Ginski. **Step 1)** By observing a star in 'pupil stabilized' mode, the field rotates with the changing parallactic angle for each subsequently recorded frame (A_i), while the pupil (illustrated with the spiders) remains fixed with respect to the detector. **Step 2)** Taking the median over all A_i frames provides a reasonable estimate of the stellar PSF (image B), while the circumstellar matter (illustrated with orange ellipses in the A_i frames) is 'averaged' out. **Step 3)** After subtracting the median frame (image B) from all the initial science frames (A_i), one is left with PSF-subtracted images (C_i), each with the circumstellar matter at a different position angle. **Step 4)** Derotating the PSF-subtracted C_i images with the parallactic angle will place north up and the circumstellar object at the same position angle on each frame D_i. **Step 5)** Median combination of the derotated images D_i leads to a higher signal-to-noise image E of the circumstellar object.

from images of the same star (observed in the same filter at approximately the same time) as the science frames, ADI is a very efficient PSF subtraction technique for the detection of planets and brown dwarfs (e.g. Marois et al. 2010). When imaging a system with strong azimuthal symmetry (e.g., a disk observed at low inclination angles) the true astrophysical signal can unfortunately get included in the reference PSF, which will result in oversubtraction of astrophysical signal. The risk of oversubtraction exists for cADI as well as ADI+PCA or

TLOCI.

In Chapter 4, we use cADI to detect companion candidates and ADI+TLOCI to image multiple rings in the disk around RX J1615.3-3255 (RX J1615). The disk is seen at inclination $i = 47 \pm 2°$, which raises the question of whether we are plagued by self-subtraction of disk signal. The comparison with PDI images allows us to constrain the shape of the disk. It is interesting to note that ADI+TLOCI seems to be very sensitive to faint disk signals at larger separations. However, the difference in seeing conditions between the pupil tracking (ADI) and polarimetric observations of RX J1615 makes it difficult to directly compare ADI with PDI in Chapter 4.

SDI Spectral Differential Imaging (SDI) requires simultaneous multi-wavelength measurements such as performed by dual-band imaging (DBI, Vigan et al. 2010) or with an Integral Field Spectrograph (IFS, Claudi et al. 2008). Our reference PSF is constructed from observations recorded at wavelength(s) different from our science frame. To perform PSF subtraction we have to take into account that speckle diffraction patterns are a function of wavelength. Therefore, we scale (interpolate) the reference image(s) before we subtract it from the science image. Alternatively, Keller & von der Luehe (1992) and Sparks & Ford (2002) describe how the reference PSF can be used to deconvolve the science image with 'speckle' or 'spectral deconvolution'.

SDI has the advantage that the reference PSF is created from observations taken simultaneously with the science frame, which is therefore affected by the exact same seeing conditions. An additional benefit of SDI is that we obtain color information on our circumstellar object. Detecting line emission of methane or Hα allows us to characterize an exoplanet atmosphere (Vigan et al. 2010) or determine whether the companion is still accreting (as illustrated for HD 142527 b, Close et al. 2014). In Chapter 4 we use DBI to characterize the companion candidates of RX J1615 using the $H2 - H3$ color.

RDI The method of reference star subtraction or differential imaging (RDI) has already been demonstrated by Smith & Terrile (1984) with their first direct detection of a circumstellar disk around β Pictoris (see Figure 1.5).

The method requires an extremely stable PSF and is therefore well-suited for space-based imagers, as was demonstrated by Soummer et al. (2012), or a very stable AO correction. In the ideal case the reference star observations yield a PSF that is extremely similar to the science target without circumstellar matter. Reference star subtraction has therefore the potential to be least plagued by self- (or over-)subtraction, which does become a large problem for low inclination disks in ADI and SDI, and for low polarization disks (due to unfavorable scattering angles or grain sizes $\gg \lambda$ Hansen & Travis 1974) in PDI. We apply RDI in

Chapter 2, where we subtract the image of a reference star (TYC5259-446-1) from recordings of our science target BP Piscium to image its nearly edge-on disk.

1.3.3 Polarimetric imaging

1.3.3.1 Polarization

When we describe a beam of light as being comprised of multiple electromagnetic waves, each wave has its own orientation of oscillation of the electric field. Polarization describes the preference of this oscillation orientation within a beam of light. A beam without a preferred orientation of oscillation (i.e., the waves oscillate in random directions), is called 'unpolarized'; while a beam for which all waves oscillate in only one direction is called 'completely (or fully) polarized'. It is possible to create a 'partially polarized' beam with a superposition of a completely polarized and an unpolarized beam.

When a beam of light propagates along the z-axis in a cartesian coordinate system within an isotropic medium, we expect the light to oscillate in the plane perpendicular to the z-axis (i.e., in the $x-y$ plane). The coherent superposition of all the waves within the quasi monochromatic beam can be described as a single oscillation that can be decomposed into x and y oscillation components. A polarized beam is called 'linearly polarized' when the x component of the oscillation is in phase with the y component (i.e., phase difference $\Delta\varphi = 0 + n \times \pi$; with $n \in \mathbb{Z}$) and 'circularly polarized' when $\Delta\varphi = \pi/2 + n \times \pi$. Any intermediate value ($n \times \pi/2 \leq \Delta\varphi \leq (n+1) \times \pi/2$) will result in an 'elliptically polarized' beam, which can be regarded as the superposition of a circularly polarized beam with a linearly polarized beam. Elliptical polarization can therefore be considered to be the generic description of polarization and linear and circular polarization are two particular cases.

Elliptical polarization (partial and full) is conveniently described by Stokes (1851) with what is known as the Stokes vector:

$$\mathbf{S} = \begin{bmatrix} I \\ Q \\ U \\ V \end{bmatrix}, \tag{1.2}$$

where I is the total intensity of the beam, Q and U describe two linear polarization contributions, and V describes circular polarization. In the literature the $+Q$ direction is often aligned with the local meridian (e.g., Witzel et al. 2011) although this choice is arbitrary. We use the following conventions for the remaining orientations. For a beam propagating in positive z direction in a right-handed x, y, z coordinate system, $+Q$ describes linear polarization with an oscillation in

the $\pm x$ direction (which we align with our prefered frame of reference, e.g., the meridian). $-Q$ then oscillates in the $\pm y$ direction; $+U$ describes linear polarization oscillating at an angle of +45° from the x-axis (rotated in counter-clockwise direction when looking at the source); while $-U$ polarized light oscillates at an angle of −45° (or +135°) with respect to the x-axis. $+V$ describes circular polarization where the peak of the electric field rotates clockwise when looking at the source (i.e. moving from $+x$ to $-y$ for a beam crossing the origin of our right-handed coordinate system); and $-V$ describes counter-clockwise rotation.

The polarimetric imaging modes of the instruments used in this thesis (the previously mentioned VLT/NACO and VLT/SPHERE/IRDIS, and SPHERE's visible light polarimeter, the Zurich IMaging POLarimeter (VLT/SPHERE/ZIMPOL) are designed to measure linear polarization only. Fortunately, linear polarization is expected to be the dominating polarization component caused by scattering at the surface layers of protoplanetary disks and exoplanets. We can determine the linearly Polarized Intensity (PI_L); Degree and Angle of Linear Polarization (DoLP or P_L & AoLP or θ_p, respectively) from the Stokes vector components according to:

$$PI_\mathrm{L} = \sqrt{Q^2 + U^2}, \tag{1.3}$$

$$P_\mathrm{L} = \frac{PI_\mathrm{L}}{I} = \frac{\sqrt{Q^2 + U^2}}{I}, \tag{1.4}$$

$$\theta_\mathrm{p} = \frac{1}{2} \arctan \frac{U}{Q}. \tag{1.5}$$

1.3.3.2 Polarimetric differential imaging

Although ideal polarimeters do not exist, such a hypothetical instrument is helpful in describing the general principles of PDI. Apart from mirrors and lenses the main components of an ideal dual-beam polarimeter are two analyzers and two detectors (or detector halfs). The analyzers can either be two separate polarizers with orthogonal polarization (also called transmission) axes or a polarizing beamsplitter[1]. Let us choose the $+Q$ direction to be aligned with the polarization axes of one analyzer (A1) and $-Q$ aligned with the other analyzer (A2). We can retrieve (or 'indirectly measure') the first two components of Equation 1.2 by combining both beams:

$$I_\mathrm{meas} = I_\mathrm{A1} + I_\mathrm{A2}, \tag{1.6}$$

$$Q_\mathrm{meas} = I_\mathrm{A1} - I_\mathrm{A2}, \tag{1.7}$$

[1] The latter splits the beam into two orthogonally polarized beams, while an analyzer with two separate polarizers (such as used by IRDIS/DPI) requires an aditional (preferably non-polarizing) beamsplitter upstream from the analyzer pair.

where $I_{A1/A2}$ are the intensities measured for the beams transmitted by A1 and A2, respectively. We can rephrase Equations 1.6 and 1.7 to describe the transmission of the analyzers:

$$I_{A1} = (I_{meas} + Q_{meas})/2, \quad (1.8)$$
$$I_{A2} = (I_{meas} - Q_{meas})/2, \quad (1.9)$$

where for an ideal polarimeter, I_{meas} and Q_{meas} will be equal to their counterparts incident on the instrument (I_{in} and Q_{in}, respectively).

To retrieve U_{meas}, we will either need to rotate the analyzer pair by 45° or introduce an optical component that can rotate the polarization direction by the same angle. A half-wave ($\lambda/2$) retarder plate (HWP) retards light that is polarized in the direction orthogonal to the fast axis with $\lambda/2$ compared to light that is polarized along the fast axis. We can use a HWP to rotate the polarization angle by $\Delta\theta_p$ by placing the fast axis of the HWP at an angle of $\Delta\theta_p/2$ with respect to the polarization axes of the analyzers (Treanor 1968). We can retrieve U_{meas} by placing the HWP at an angle $\theta_{hwp} = 22.5°$ with respect to the polarization axis of A1 (Equation 1.7 will now yield U_{meas}), which changes Equations 1.8 and 1.9 into: $I_{A1/A2} = (I_{meas} \pm U_{meas})/2$. We now see why the Stokes vector notation is convenient: its components are easily retrieved from the observables of an ideal polarimeter, which 'measures' a Stokes vector ($\mathbf{S}_{meas}$) unaltered by the telescope and instrument (i.e. $\mathbf{S}_{meas} = \mathbf{S}_{in}$, where $\mathbf{S}_{in}$ is the incident Stokes vector).

Real polarimeters are never ideal. Reflecting (and to a lesser degree even transmitting) surfaces of the telescope and instrument will introduce polarization unrelated to the astrophysical signal, called telescope and instrumental polarization (*IP*). Therefore, it is a common practice to adjust the observing strategy to remove *IP* downstream from the HWP by recording Q_{meas} with two HWP angles: $\theta_{hwp} = 0° \,\&\, 45°$ (see e.g. Canovas et al. 2011, Tinbergen 1996, Witzel et al. 2011). Because the second θ_{hwp} changes the signs in Equations 1.8 & 1.9, we change the notation of Equation 1.7 to measure $Q^+_{meas} = Q_{meas} + IP$ for $\theta_{hwp} = 0°$; and $Q^-_{meas} = -Q_{meas} + IP$ for $\theta_{hwp} = 45°$. We can apply the *double difference* method to obtain the *IP*-corrected Stokes parameters.

$$Q_{meas} = (Q^+_{meas} - Q^-_{meas})/2, \quad (1.10)$$
$$U_{meas} = (U^+_{meas} - U^-_{meas})/2, \quad (1.11)$$

where $U^+_{meas}(= U_{meas} + IP)$ and $U^-_{meas}(= -U_{meas} + IP)$ are measured with $\theta_{hwp} = 22.5°$ and 67.5°, respectively. Alternatively, one can use the *double ratio* method, as described by Semel et al. (1993). However, we have found no significant benefit in using the double ratio, rather a slightly worse performance at lower signal-to-noise measurements (similar to the results of Canovas et al. 2011). Therefore, we stick for the remainder of this study to using the double difference method.

1.3.3.3 Polarimetry as a characterization method

Apart from being an effective high-contrast technique, polarimetry has the potential to characterize scattering particles (e.g., particle shape and size distribution) in circumstellar disks and planets. Radiative transfer modeling of disks is heavily plagued by degeneracy when they are based on the Spectral Energy Distribution (SED) alone (e.g. Andrews et al. 2011, Dong et al. 2012). Milli et al. (2015) have used the resolved polarimetric surface brightness to determine the polarization phase function for the debris disk around HR 4796A. The polarization phase function (component [2,1] of the 4x4 phase matrix Hansen & Travis (1974), describing how the polarization of unpolarized incident light depends on scattering angle) will be instrumental in the unambiguous characterization of micron-sized dust particles.

1.4 Outline of this thesis

The work discussed in this thesis focuses on high-contrast observations of protoplanetary disks. It is necessary for a reliable analysis of these data that we thoroughly understand the instruments with which the observations are performed. Therefore, the chapters in this thesis can be divided into the following two topics. I have worked on the astrophysical interpretation of high-contrast imaging data of protoplanetary disks and on the characterization of the polarimetric modes of high-contrast imagers. The VLT/SPHERE observations of BP Piscium, J1604, and RX J1615 are discussed in Chapters 2, 3 and 4, respectively. In Chapters 5 and 6, we have characterized the polarimetric modes of VLT/NACO and VLT/SPHERE/IRDIS, respectively.

In Chapter 2 we describe how we imaged the disk of BP Piscium with polarimetric observations recorded with SPHERE/ZIMPOL during the instrument's science verification time. The literature is not conclusive about the evolutionary stage of BP Piscium: either it is a Classical T Tauri Star (pre-main sequence) at ~ 80 pc; or it is a first ascent G-giant (post-main sequence) at ~ 300 pc. However, it is known to be surrounded by a gas and dust disk, which would be very peculiar for a post-main sequence star during its hydrogen shell burning phase. Our simple radiative transfer models explain both the ZIMPOL images and the SED of the star and are incongruent with typical pre-main sequence systems.

The visible-light SPHERE/ZIMPOL polarimetric observations of J1604 are described in Chapter 3. We detect a circumstellar disk with a wide gap surrounded by a clear ring-like structure in the scattering surface of the disk. We compare the disk-annulus, which has an azimuthal asymmetry (dip) in the northeast, with the previous detections of the annulus by Subaru/HiCIAO (in NIR) and ALMA (sub-mm). We find that the peak in the radial brightness profile

moves outward with wavelength, which is consistent with dust filtration at the edge of a gap caused by a massive planet. The dip in the disk-annulus detected in the ZIMPOL data has a different position angle (PA) than the HiCIAO image recorded three years prior to our ZIMPOL observations. This variability in the disk surface brightness cannot be explained by an azimuthal asymmetry in the density of the annulus, rotating at Keplerian velocity. Instead, we suggest that the dip is caused by an object closer to the star that casts a shadow onto the outer disk, and we place upper limits on the orbital period of the shadow-casting object.

In Chapter 4, we present the SPHERE consortium Guaranteed Time Observations of the classical T Tauri star RX J1615. We applied Angular Differential Imaging on SPHERE/IRDIS pupil tracking data, which resulted in the detection of nine point sources and an inclined ($i = 47 \pm 2°$) disk with multiple elliptical rings in its scattering surface. We revisited archival VLT/NACO data and detected four of the nine potential companions, which turned out to be not co-moving with RX J1615, and are therefore no longer considered as companion candidates. We also imaged the disk with the polarimetric modes of SPHERE/IRDIS and SPHERE/ZIMPOL. Due to the low R-band brightness ($R = 11.2$ mag) and poor seeing conditions, we marginally detected the disk in the ZIMPOL data. The IRDIS/DPI data is noisier than the IRDIS/ADI data. However, the DPI image allowed us to confirm that the general shape seen in the ADI data is not caused by self-subtraction, but traces the surface of the disk. The DPI data also shows an inner cavity in the disk. We measure apparent offsets for the multiple ellipses with respect to the star-center, which we explain as a projection of concentric circular rings due to the disk inclination. The offsets become apparent because the scattering surfaces of the rings lie on planes parallel to, yet above and below the mid-plane, which contains the star. We use this offset for the first ever model-independent determination of the scattering surface height.

For the polarimetric characterization of VLT/NACO in Chapter 5 we used the polarized skylight by looking at zenith during twilight. The polarization angle of skylight can be determined from the position of the Sun during the observations and certain telescope and instrumental polarization and crosstalk terms cancel out when we perform a 'double difference' between two observations taken with the telescope or instrument (component) rotated by 90°, while other instrumental effects remain. Rotating all the individual optical components (including Unit Telescope 4) by 90° allowed us to disentangle the instrumental effects due to the different components.

The calibration of the polarimetric mode of VLT/SPHERE/IRDIS in Chapter 6 is performed by observing the internal light source with and without the calibration polarizer inserted and by observing unpolarized standard stars for an extended range of parallactic angles. The internal light source observations were

taken with different derotator and HWP angles, which allowed us to calibrate the retardance and diattenuation of these optical components. Our newly acquired knowledge of the optical components downstream from SPHERE's first reflective surface (M4), combined with the observations of unpolarized standard stars allowed us to determine the diattenuation of both the tertiary mirror (M3) of Unit Telescope 3 and M4. We have validated our calibrations by explaining and correcting the instrumental effects seen in the IRDIS/DPI observations of TW Hydrae.

1.5 Future directions

Recent imaging observations of protoplanetary disks at high angular resolution, in both scattered light (VLT/NACO, Subaru/HiCIAO, Magellan/MagAO, Gemini/GPI, VLT/SPHERE) and sub-mm interferometry (Plateau de Bure, ALMA) have yielded a wealth of information on grain properties and spatial distributions of dust. Variability in disk surface brightness has only been detected for very few disks (e.g., Chapter 3 and Stolker et al. 2016), but is still poorly understood. Therefore, surface brightness variability should be investigated more extensively and for a larger number of disks. In the near future, much effort will be put into simultaneous radiative transfer modeling of both scattered light and sub-mm imaging data of disks. We have already found substantial differences between ALMA and SPHERE images (e.g., Chapter 3), which teach us about detailed physical processes acting within disks such as dust trapping at pressure maxima.

Kataoka et al. (2016) have recently detected the sub-mm polarization with ALMA in the protoplanetary disk of HD 142527 and concluded that self-scattering of thermal dust emission can trace dust density gradients. Creating models that can explain both sub-mm polarimetric images with NIR scattered light images will become an important focus point for theorists. New information will also come from the fact that we are just starting to understand our cutting-edge polarimeters (see Chapter 6) on a level that allows accurate measurements of degrees and angles of polarization. The polarization angle will allow us to recognize multiple-scattering in the disk, which together with the polarization degree will enable the construction of more sophisticated radiative transfer models, better suited to determine the grain properties such as dust settling towards the mid-plane and grain size distributions (Perrin et al. 2015).

To our surprise, we detect far fewer planets than was expected (Beuzit et al. 2006) before the commissioning of extreme AO assisted high-contrast imagers. To solve this problem, better calibration schemes will be useful, but more is to be expected from the improvement of existing high-constrast imagers, for example

with superior AO systems (e.g., pyramid WFS, Esposito & Riccardi 2001) and coronagraphs (e.g., vAPP, Otten et al. 2017).

The most exciting developments are likely to come from future telescopes such as the James Webb Space Telescope (JWST, scheduled to launch in October 2018) and the European Extremely Large Telescope (EELT, first light expected in 2024). The enhanced sensitivity and the opportunity for especially Mid-IR (MIR) imaging and spectroscopy with these telescopes will boost our knowledge on protoplanetary disks. Determining the spatial distribution of different species of Polycyclic Aromatic Hydrocarbons (which emit mostly at MIR wavelengths) might teach us about the difference between Herbig Type I and Type II disk geometry (Maaskant et al. 2013). JWST/MIRI will allow us to observe star formation at younger stages than currently possible, and detect disks when they are still embedded (Rieke et al. 2015). Higher sensitivity at longer IR wavelengths will be crucial to answer the very urgent question of what sculpts the cavities and gaps in (pre)transitional disks. The expected high sensitivities for the instruments of JWST make this telescope our best option to detect young planets within their native environment within the next few years.